Mechanical stretching of 3D hydrogels for neural stem cell differentiation

Quanjing Mei, Ho-Yin Yuen, Xin Zhao

Department of Biomedical Engineering, The Hong Kong Polytechnic University, Hung Hom, Hong Kong, China
*Correspondence to: Xin Zhao, Department of Biomedical Engineering, The Hong Kong Polytechnic University, Hung Hom, Hong Kong, China; Email: xin.zhao@polyu.edu.hk

Abstract

While it is known that mechanical dynamics are influential in neural differentiation for critical processes like neurogenesis or neurodegeneration, studies on neural stem cell therapies usually focus on biochemical interactions rather than mechanical aspects, frequently resulting in low efficacy and unfulfilled potential. Therefore, current studies are attempting to elucidate the effect of mechanical stimulus on neural performance using conventional two-dimensional (2D) planar substrates. Yet, these 2D substrates fail to capture the defining three-dimensional (3D) characteristics of the in vivo neural stem cell environment. To complete this research gap, we synthesized a series of soft and elastic 3D hydrogels to mimic the neural tissue mechanical environment for 3D cell culture, using long-chain polyethylene glycol diacrylate (PEGDA) and gelatin-methacryloyl (GelMA). By varying the concentration of the polymer, we obtained biomimicking hydrogels with a tensile modulus as low as 10 kPa and a compressive modulus as low as 0.8 kPa. The in vitro results demonstrated that GelMA-PEGDA hydrogels have the high biocompatibility required to support neural cell growth, proliferation, and differentiation, as well as neurite outgrowth. We then studied the effect of mechanical stretching on the behaviors of neural cells and observed that mechanical stretching could significantly enhance neurite extension and axon elongation. In addition, the neurites were more directionally oriented to the stretching direction. Immunocytochemistry and relative gene expression data also suggested that mechanical tension could upregulate the expression of neural differentiation protein and genes, including GFAP and βIII-Tubulin. Overall, this study shows that in addition to the specific mechanical properties of GelMA-PEGDA that improve neural differentiation towards specific lineages, hydrogel stretching is also a potentially attractive strategy to improve the therapeutic outcomes of neural stem cell therapies.

Keywords: Mechanical property, Tensile stretching, Hydrogels, Neural differentiation, 3D cell culture

Graphic abstract:
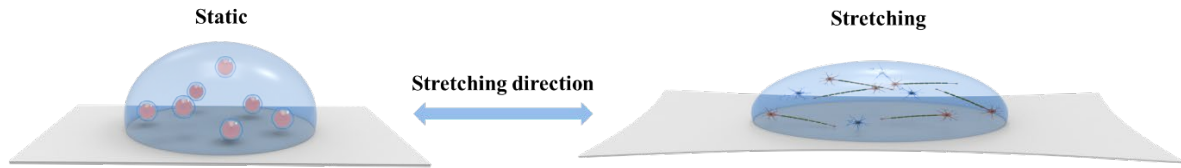
1. Introduction

Due to the long-lived nature and low turnover of neural cells [1], having their differentiation to be committed into the proper neural lineage is extremely important for neurogenesis and many other functions. Among factors that affect differentiation, the mechanical characteristics of the neural microenvironment are perhaps the most critical yet unclear mechanisms, by which the neural cells differentiate under the influence of both the varying stiffness [2] and cortex terrain that elongate the cells [3]. This unclear understanding hinders emerging neural treatments like neural stem cell transplantation [4], in which securing differentiation under appropriate mechanical conditions is crucial and failure to do so would be tumorigenic [5]. Therefore, various preliminary studies have characterized some aspects of mechanical neural differentiation [6] via the use of micropatterned substrates [7, 8], material stiffness [9, 10], or material stretching [11]. However, these studies usually investigate the effects on conventional two-dimensional (2D) substrates instead of three-dimensional (3D) scaffolds due to the lack of materials with soft elasticity. Harder materials fail to capture the in-vivo conditions and hence provide less explanatory power with regard to the underlying mechanisms.

Neural tissue is one of the softest tissues in the body [12, 13], with moduli about 1–4 kPa for brain [14-20] and moduli about 0.50–6.63 kPa for spinal cord [21-23]. To mimic the stiffness of natural neural tissues, we fabricated a series of soft and elastic hydrogels using a mixture of gelatin-methacryloyl (GelMA) and high molecular-weight polyethylene glycol diacrylate (PEGDA) to induce neural differentiation. Although GelMA and PEGDA have different sources, chemical structures, and physical properties, they both have high biocompatibility, with multiple applications in cell encapsulation [24-26], stem cell transplantation [27-29], and tissue engineering [30-33]. In particular, while GelMA has short photo-crosslinking chains and hence high matrix rigidity and low flexibility [34], it has outstanding biocompatibility due to its similar composition to the extracellular matrices [35], and is rich in cell-adhesive peptides for differentiation [36]. On the other hand, while high molecular-weight PEGDA lacks cell-adhesive peptide, it has a linear and long-chain molecular structure and hence high elasticity. By changing the ratio of GelMA and PEGDA hydrogels, we constructed a series of lifelike tissues to recapitulate the properties of native neural tissue.

These hybrid GelMA-PEGDA hydrogels allowed us to investigate two major aspects of neural differentiation: firstly, the hydrogel provided a biocompatible, soft, and encapsulated 3D environment that mimicked the low stiffness of neural tissues [20] (approximately 1–7 kPa for neuronal differentiation [37]); secondly, stretching the hydrogels mimicked the morphological changes that closely resemble the dynamics in the brain for neural differentiation both at the cellular level (e.g., stretch-activated ion channels for neural differentiation [38]) and the tissue

level (e.g., cell elongation during neural tube formation [39]). Furthermore, since traditional stretching setups are unsuitable for long-term observation and micro-manipulation, we developed a simple and reproducible neural stretching system by crosslinking the cell-laden hydrogel onto a plasma-treated elastic membrane and then stretching the membrane alongside the hydrogel. This design would enable us to transfer stable strain and stress to the encapsulated cells effectively.

We envision that showing this design of hybrid hydrogels that influence neural differentiation in both 3D encapsulation and mechanical stretching could inspire novel strategies in neuronal regenerative medicine utilizing the mechanical properties of soft materials.

The paper is organized as follows. We first describe the synthesis of a series of GelMA-PEGDA hydrogels with varying concentrations. Then, we discuss the effects of the mechanical properties and our experiments with stretched hydrogels.

2. Materials and methods

2.1 GelMA and PEGDA synthesis

Gelatin (Type A, Sigma-Aldrich) was modified by covalent immobilization of methacrylate anhydride (MA, Sigma-Aldrich) via amide reaction [29, 40]. In brief, gelatin (300 mg) was dissolved in phosphate buffer solution (PBS, HyClone, pH=7.4) (30 mL) and the mixed solution was stirred at 50 °C for 30 min. MA (0.03 mL) was added into the gelatin solution dropwise at a stirring rate of 500 rpm. The solution was maintained at 50 °C for 2 h. After filtration, the solution was dialyzed with 50 °C water and freeze-dried. The substitution degree of the resultant GelMA was determined by nuclear magnetic resonance spectroscopy (^{1}H-NMR) (JEOL ECZ500R 500 MHz), based on previous work [29, 40].

PEGDA was synthesized by the reaction between the hydroxyl group on polyethylene glycol (PEG, 20 kDa, Sigma-Aldrich) and the carboxyl group on acryloyl chloride (Sigma-Aldrich) [41]. Briefly, 10 wt% PEG was dissolved in dichloromethane by stirring for 30 min. Then acryloyl chloride and triethylamine (Sigma-Aldrich) were added gradually and separately to the above solution. The molar ratio of PEG, triethylamine, and acryloyl was 1:4:4. Under N_2 protection, the mixture was stirred overnight. After reaction, ice-cold ether was added to precipitate the preliminary product. The product was further purified by rotary evaporation and dialyzed to eliminate by-products, then freeze-dried. The structure of PEGDA was also confirmed by ^{1}H-NMR.

The hybrid hydrogels were prepared by dissolving varying amounts of freeze-dried GelMA and PEGDA macromer with 0.5 wt% photo-initiator lithium phenyl-2,4,6-trimethylbenzoylphosphinate (LAP, Sigma-Aldrich). The mixed hydrogel was photo-crosslinked with Ultraviolet (UV) light (360–480 nm) at an intensity of 6.9 mW/cm^2 for 20 s.

2.2 Mechanical testing

Compression and tensile tests were performed on a mechanical tester (Instron, USA). For tensile tests, hydrogel samples with a dimension of 30 mm × 10 mm × 3 mm (length×width×height) were loaded on the mechanical tester. The cyclic tensile test was performed by reloading immediately after the initial loading–unloading trial based on

previously reported procedures [42, 43]. The specimens (length 30 mm, width 10 mm, and height 3 mm) were stretched to a maximum strain of 50% for 100 cycles. For the compression test, cylindrical samples (d=10 mm, h=5 mm) were prepared and tested on the same machine. All experiments were carried out at room temperature at a speed of 0.5 mm/min according to the established protocol [40]. Compressive modulus and tensile modulus were calculated by linear fitting of stress−strain curves between 0 and 10%.

2.3 Swelling experiment

The swelling test was conducted on cylindrical samples (d=10 mm, h=3 mm) at room temperature to evaluate the effects of crosslinking on the hydrogels [40]. By measuring the weight change of samples immersed in PBS at different time points, we were able to determine the swelling characteristics of the hydrogels. The swelling ratio was calculated using the formulation below:

$$\text{Swelling} = \left(\frac{W_s - W_i}{W_i}\right) \times 100\%, \qquad (1)$$

where W_s and W_i are the wet weights at the end and initial time points, respectively.

2.4 Viscosity test

The viscosity tests for hydrogels of different compositions were performed on an MCR 702 rheometer equipped with temperature-controlling systems, using a 25-mm-diameter parallel plate. The viscosity of the hydrogel solutions was measured using the shear rate from 0.1 to 1000 s^{-1} at 37 °C.

2.5 Degradation of hydrogel

To investigate the connection between hydrogel composition and degradation properties, we immersed the swollen hydrogels (d=10 mm, h=3 mm, after 12 h immersion in deionized water) in 2 mL of 0.2 U/mL collagenase type II solution (Sigma-Aldrich) at 37 °C [44]. The collagenase solution was replaced every 2 days to maintain enzyme activity. We removed hydrogel samples from the collagenase solution and weighed them at predetermined time points. The degradation property of hydrogels was determined using the following equation [45]:

$$\text{Mass remaining} = \left(\frac{W_t}{W_0}\right) \times 100\% \qquad (2$$

where W_0 represents the initial weight (equilibrium swelling weight) of the hydrogel and W_t represents the remaining wet weight of the hydrogel after collagenase incubation at different time points.

2.6 Cell culture

Mouse neuroblastoma cell line Neuro2a (N2a, ATCC, USA) was used in this project. This cell line has been extensively used in studies of neuronal differentiation, axon growth, and signaling pathways [46]. N2a cells were cultured as described in previous work with a complete growth medium (89% Dulbecco's Modified Eagle Medium (DMEM) high glucose + 1% penicillin-streptomycin solution + 10% fetal bovine serum FBS). For differentiation of N2a, a differentiation medium (98% DMEM-high glucose + 1% penicillin-streptomycin solution + 1% FBS +10 μM retinoic acid) was used [47]. The medium was replaced every 2 days during the

4

incubation period.

2.7 Cell culture on 2D hydrogel

The precursor hydrogel solution with 0.5 wt% LAP was filtered through a 0.22-µm filter for sterilization. 150 µL of hydrogel was pipetted to each hole of a 12-well plate and the plate was placed into a 37 °C incubator for 10 min to spread the hydrogel to the entire area. After that, the hydrogel was crosslinked for 20 s under UV at an intensity of 6.9 mW/cm^2 (360–480 nm). Following hydrogel crosslinking, N2a suspensions (1×10^5 cells/mL) were seeded on top of the hydrogel at a density of 1×10^4 cells/cm^2 and left to adhere overnight. For cell viability and proliferation, the complete growth medium was applied, while for cell differentiation of N2a, a differentiation medium (98% DMEM-high glucose + 1% penicillin-streptomycin solution + 1% FBS + 10 µM retinoic acid) was used.

2.8 Cell encapsulation in hydrogel and stretching the 3D hydrogel system

N2a cells were encapsulated in precursor hydrogel at a density of 1×10^6 cells/mL. We dripped 10 µL of cell-loaded hydrogel solution onto the plasma-treated rubber bands. After UV photo-crosslinking for 20 s at an intensity of 6.9 mW/cm^2 (360–480 nm), the cell-laden hydrogel that was sitting on the rubber band could be crosslinked onto it. To prepare the 3D stretching system, we used a glass cutter to cut three different lengths of glass for each stretching proportion (i.e., initial length=24 mm; 25% stretching=30 mm; 50% stretching=36 mm). Then, we tied and fixed the plasma-treated rubber bands on some initial-length pieces of glass slide and dripped 10 µL of cell-loaded hydrogels suspension onto the rubber bands. After photo-crosslinking, we stretched the rubber bands so that the corresponding hydrogel was also stretched alongside the rubber band, and we subsequently fixed them onto the glass of a specific length so that the rubber bands (and hydrogel) stayed at a stretching ratio of either 25% or 50%. A video showing the 3D stretching hydrogel system is provided in the supporting information (Video S1). The prepared glass and rubber bands were sterilized by autoclave before use.

2.9 Cell viability, proliferation, and morphology characterization
2.9.1 Cell viability

For cell viability evaluation, we conducted a live/dead assay (Thermo Fisher, Hong Kong, China) by following instructions from the manufacturer. Briefly, a certain amount of live/dead solution (4 mmol/L ethidium homodimer-1 and 2 mmol/L calcein AM in PBS) was added to each sample and incubated for 30 min at 37 °C. After washing with PBS, the samples were examined with a fluorescence microscope (Nikon, Japan).

2.9.2 Cell proliferation

Cell counting kit-8 (CCK-8, Sigma Aldrich) was used to measure in vitro cell proliferation according to the manufacturer's instructions. CCK-8 solution was added to each well and incubated for 2 h on days 1, 3, and 5 of culture. The optical density (OD) was detected by a microplate reader (Bio-Rad 550, California, USA) at 450 nm.

2.9.3 Cell morphology

The cells were fixed with 4% paraformaldehyde for 20 min, then permeabilized with 0.1% Triton X-100 for 20 min and blocked for 45 min using 1% bovine serum albumin (BSA) at room temperature. Subsequently, samples were incubated in Alexa Fluor 488-conjugated phalloidin solution (Thermo Fisher, Hong Kong, China) (1:200 dilution) for 45 min and DAPI solution (Thermo Fisher, Hong Kong, China) (1:1000 dilution) for another 5 min in the dark. After washing samples with PBS three times, we examined them by fluorescence microscopy.

2.10 Immunocytochemistry

For immunostaining, hydrogel specimens were also fixed in 4% paraformaldehyde for 20 min. Then the samples were permeated in 0.1% Triton X-100 for another 20 min. After incubation with 1% BSA for 45 min, samples were incubated in a mixture of two primary antibodies (rabbit anti-GFAP 1:500 and mouse anti-β-Tubulin 3 1:500) (Abcam, UK), in primary antibody diluent overnight at 4 ℃. After primary antibody binding, the samples were incubated in a mixture of two secondary antibodies (Goat pAb to Rb 488 FITC-conjugated; 1:500; Goat pAb to Ms 594 Red conjugated 1:500) (Abcam, UK) in secondary antibody dilution for 2 h at 37 ℃ in the dark. Finally, samples were stained with DAPI solution (1:1000 dilution) for 5 min at 37 ℃.

2.11 Gene expression

Gene expression was detected by the reverse transcription quantitative polymerase chain reaction (RT-qPCR), based on the literature [48]. After culturing cells on 2D hydrogel for different lengths of time, they were collected by trypsinization. For 3D hydrogels that encapsulated cells, we used collagenase type II (Sigma-Aldrich) to digest the hydrogels and release the encapsulated cells. Total RNA was extracted from the collected N2a cells using a Total RNA Kit (Omega, Hong Kong, China), and was reverse transcribed into complementary DNA (cDNA) using the Prime Script RT Master Mix Kit (Takarabio, Hong Kong, China). We used GAPDH as an internal control for normalization. The sequences of the sense and antisense primers for related genes are provided in Table 1. The $2^{-\Delta\Delta C_t}$ method was used to calculate gene expression.

Table 1 Primer sequence for RT-qPCR

Target	Sequence (5'- 3')
GAPDH	F: GCTGGAGGGCGAAGAAAAC
GAPDH	R: GCCTTCTGACACGGATTTGG
Nestin	F: AAGTTCCCAGGCTTCTCTTG
Nestin	R: GTCTCAAGGGTATTAGGCAAGG
GFAP	F: GCTGGAGGGCGAAGAAAAC
GFAP	R: GCCTTCTGACACGGATTTGG
Tuj1	F: ACCCCGTGGGCTCAAAAT
Tuj1	R: CCGGAACATGGCTGTGAACT

2.12 Statistical analysis

The statistical analysis was performed with SPSS software. Unless otherwise stated, all tests were repeated in triplicate. Results were presented as mean±standard deviation (SD). A normality test was conducted for each set of data, showing whether the data followed a normal

distribution. We adopted the two-tailed Student's T-test to compare the two different groups; $^*p \leq 0.05$, $^{**}p \leq 0.01$, and $^{***}p \leq 0.001$ indicate statistically significant differences.

3. Results and discussion
3.1 Physical and chemical characterization of hydrogels
First, we characterized the synthesis of GelMA by ^{1}H-NMR (Fig. 1a). The appearance of the vinyl group at about 5.64 and 5.36 ppm (1 ppm=1×10^{-6}) confirmed successful grafting of MA onto the gelatin. Meanwhile, the increase in the methyl peak at 1.9 ppm and the decrease in the peak at 2.9 ppm (the protons of methylene of lysine) also confirmed the modification of MA. The degree of substitution (DS) was calculated as 90% by changes in the peak area of lysine methylene protons (2.9 ppm) on the gelatin and GelMA [40]:

$$DS = \left(1 - \frac{I_1}{I_2}\right) \times 100\% \qquad (3)$$

where I_1 and I_2 represent the integrated area of lysine methylene on GelMA and gelatin, respectively. We also examined the synthesis of PEGDA with ^{1}H-NMR. As shown in Fig. 1b, compared with PEG, characteristic peaks of the acrylate group were observed at 5.8, 6.1, and 6.4 ppm, confirming successful synthesis of PEGDA. Meanwhile, the peak at about 4.3 ppm was identified as representing the ether groups ($-CH_2OCO-$) in the PEGDA molecular structure [49, 50].

Since the mechanical properties of hydrogels have a significant influence on the growth and differentiation of nerve stem cells, we fabricated hydrogels with different compositions and mechanical properties (Figs. 1c–1j). The three different compositions are annotated as follows: G for 5 wt% GelMA, G:P=4:1 for 4 wt% GelMA + 1 wt% PEGDA, and G:P=2.5:2.5 for 2.5 wt% GelMA + 2.5 wt% PEGDA. All hydrogels showed a typical linear elastic performance at low stress. Initially, we investigated the changes in tensile performance with different compositions. As can be seen from Figs. 1c–1e, incorporation of PEGDA significantly improved the elongation at break. Of the three compositions, the G:P=2.5:2.5 group had the largest elongation (about 180%), followed by the G:P=4:1 group (about 150%) and lastly the G group (about 60%). As the ratio of PEGDA increased, the tensile stress and tensile modulus of the composite hydrogels significantly decreased from ~60 kPa (5 wt% GelMA) to about 10 kPa (G:P=2.5:2.5). We then performed the cyclic tensile test on the hydrogel samples. The typical stress−strain curves for different runs (1st cycle, 10th cycle, and 100th cycle) are shown in Figs. 1f–1h. All hydrogels exhibited excellent tensile recoverability after 100 loading–unloading cycles, demonstrating the outstanding stretchability of hydrogels. Hysteresis, a feature of viscoelastic materials, was also observed in these cyclic tensile curves [42, 51]. When the hydrogels were stretched to the same strain several times, a hysteresis loop with a small residual strain could be seen in the 1st loading–unloading cycle to the 10th cycle, and hysteresis reached a steady state with much less significance for the 10th to 100th cycles. These cyclic tensile results demonstrated that all hydrogels had stretchability and recoverability for application of stretching stimulation. Compared with pure GelMA hydrogel, incorporating PEGDA significantly moderated tensile strength and improved the stretchability of the hydrogel matrix. Additionally, incorporating long-chain PEGDA decreased the compression stress and modulus from ~6 kPa (5 wt% GelMA) to 0.8 kPa (G:P=2.5:2.5), as shown in Figs. 1i and 1j. Since neural differentiation is usually favorable with stiffness ranging from 1 to 10 kPa, our hydrogels are

considered suitable to mimic the physiological microenvironment [37].

Because the swelling behavior reflects the hydrogel crosslinking performance and has an important influence on the mechanical properties, this was also tested and is shown in Fig. 1k. We found that the swelling reached equilibrium after 9 h soaking in PBS. The swelling ratio increased with the increase of PEGDA, and the PEGDA: G:P=2.5:2.5 group showed the largest swelling ratio (about 80%), while the GelMA group showed the smallest swelling ratio (about 8%). These results were consistent with our expectation: incorporation of high-molecular-weight PEGDA modulated the stiffness, elongation, and swelling of hydrogels due to the increased chain flexibility and changes in the cross-linked network structure [52-54].

Viscosity, like many other mechanical properties, also influenced cellular behaviors. Primarily, viscosity affects cell behavior due to structural reorganization of the matrix [55, 56]. To evaluate whether the viscosity of GelMA-PEGDA hydrogels is suitable for neural-cell encapsulation, growth, and differentiation, we tested the viscosity of hydrogels of different compositions with the MCR 702 rheometer using the shear rate from 0.1 to 1000 s^{-1} at 37 °C (Fig. S1 in Supplementary Information). Results showed that all hydrogels exhibited similar shear-thinning properties. As the proportion of PEGDA increased, the viscosity of the composite hydrogels decreased slightly from 6.8 mPa·s to 4.7 mPa·s, similar to the viscosity of neural extracellular matrix (ECM) derived hydrogels with proven capability for cell survival [57].

The degradation results of different hydrogels in collagenase solution are shown in Fig. S2 (Supplementary Information). The hydrogels with higher PEGDA concentrations degraded faster than pure GelMA hydrogel, with full degradation by 50 h for the G:P=2.5:2.5 group and 80 h for the G group. Generally, traditional PEGDA hydrogel is susceptible to slow degradation [58]. However, the high molecular weight and low concentration could significantly accelerate hydrolysis of PEGDA hydrogel due to higher ratios of hydrolysable esters and lower crosslink density [59]. Meanwhile, enzymatic degradation of the GelMA network accelerated hydrolysis of PEGDA, resulting in rapid degradation of GelMA-PEGDA hydrogels. Although the weak crosslinking network shortened degradation time, it endowed the hydrogel with soft and flexible properties for cell survival and application of mechanical stimulation.
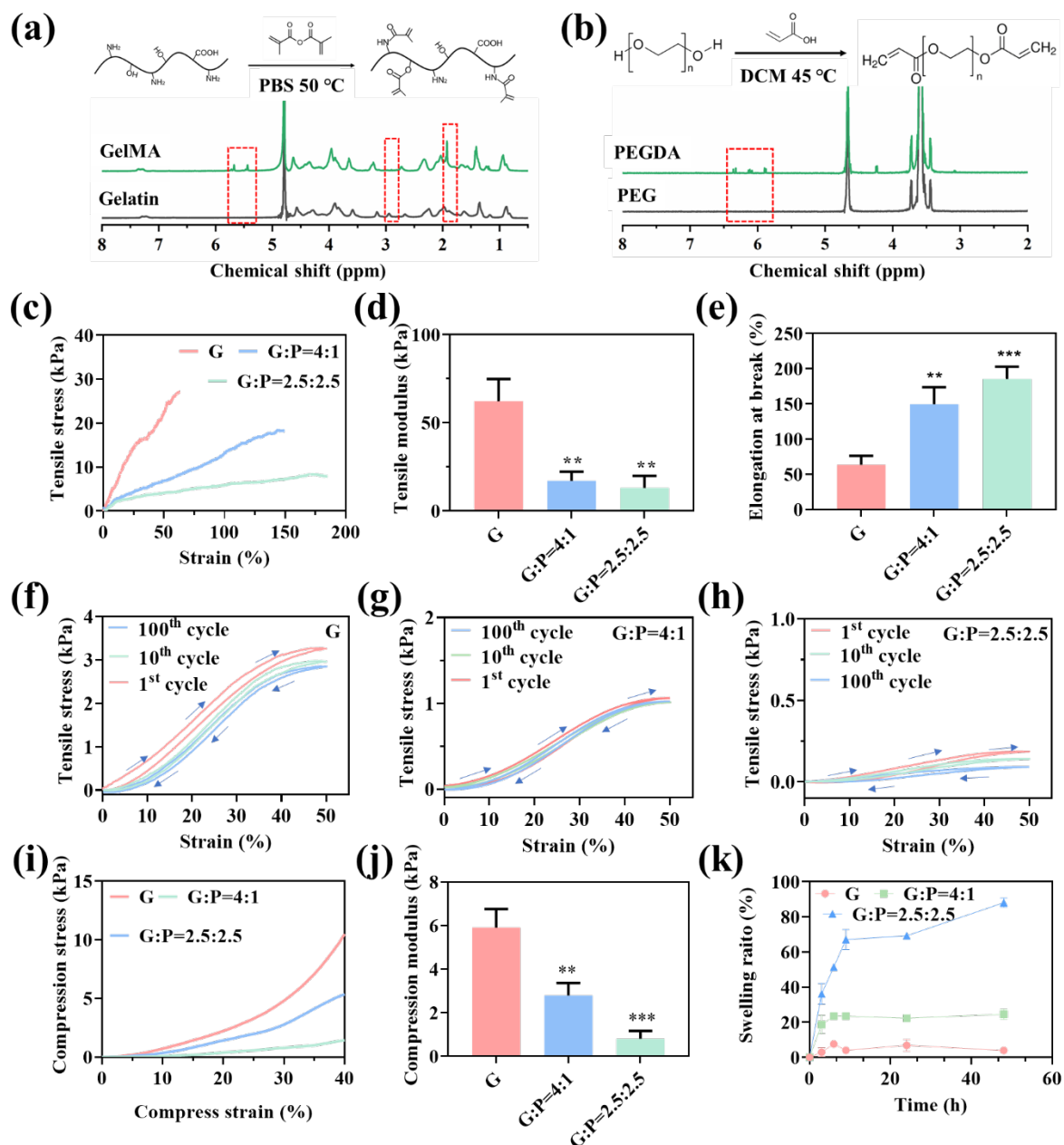
Fig. 1. Synthesis and physical characterization of hydrogels. (a) Schematic of GelMA synthesis with ^{1}H NMR spectra of gelatin and GelMA. (b) Schematic of PEGDA synthesis with ^{1}H NMR spectra of PEG and PEGDA. (c, d) Tensile properties of hydrogels. (e) Elongation at break of hydrogels. Cyclic tensile-stress curves of G (f), G:P=4:1 (g), and G:P=2.5:2.5 (h) hydrogels. (i, j) Compression properties of hydrogels. (k) Swelling properties of hydrogels. G represents 5 wt% GelMA, G:P=4:1 represents 4 wt% GelMA+1 wt% PEGDA, and G:P=2.5:2.5 represents 2.5 wt% GelMA+2.5 wt% PEGDA. 1 ppm=1×10^{-6}

3.2 Cell viability and proliferation on 2D hydrogels

To verify the feasibility of GelMA-PEGDA hydrogels for neural-tissue engineering, we evaluated the cell viability and proliferation of N2a cells on 2D hydrogels. We determined the viability of cells on the hydrogels by live/dead staining and used N2a cells cultured on a 12-well plate as control. As can be seen in Figs. 2a and 2c1, the cells were highly viable, and no

significant cytotoxicity was found. The cells remained 90% viable after 1 and 5 days of culture. The N2a cells were also uniformly dispersed onto the hydrogels as in the control samples, indicating the excellent cytocompatibility of our hydrogels.

To observe the morphology of N2a cells on hydrogels, we used phalloidin/DAPI to stain N2a cells, resulting in cell nuclei stained in blue and actin filaments in green (Fig. 2b). N2a cells were spherical and distributed evenly on day 1. After 5 days of cultivation in complete growth medium, the number of cells increased significantly, but most cells remained undifferentiated and had a round morphology. The proliferation of N2a was further evaluated with CCK-8 (Fig. 2c2). After 5 days of culture, we found that the control group (on tissue culture plastic) had the fastest growth, followed by the G and G:P=4:1 groups. Cells in the G:P=2.5:2.5 group had the lowest proliferation, possibly due to the high ratio of PEGDA, which is short of biological ligands (e.g., RGD peptides) to engage cell surface receptors for cell adhesion and proliferation [60].
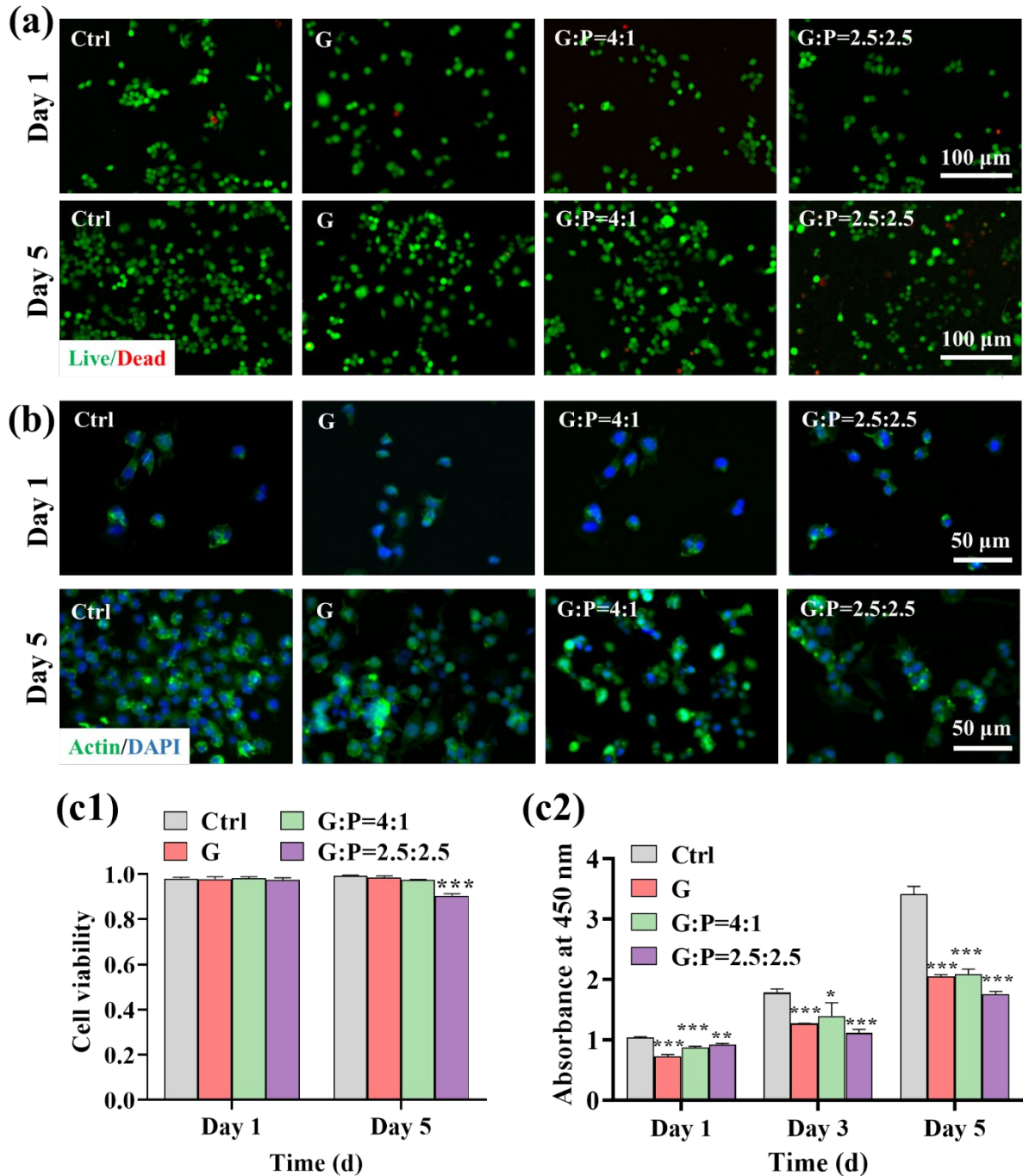
Fig. 2 Viability and proliferation of N2a on 2D hydrogels. (a) Live/dead staining of N2a on day 1 and day 5. (b) Cell morphology of N2a by F-actin staining on day 1 and day 5. (c1, c2) Cell viability and proliferation at different times. Ctrl: N2a cultured on a 12-well plate; G means 5 wt% GelMA; G:P=4:1 means 4 wt% GelMA+1 wt% PEGDA; G:P=2.5:2.5 means 2.5 wt% GelMA+2.5 wt% PEGDA.

3.3 Cell differentiation on 2D hydrogels

After showing that the hydrogels had good cytocompatibility, we further used the differentiation medium to induce neural differentiation on 2D hydrogels. First, phalloidin/DAPI staining was used to observe the morphology of N2a cells before and after differentiation on day 1 and day

11

5. As in the previous experiments, N2a cells cultured in a 12-well plate were used as control. Fig. 3a shows that the cells were spherical and did not spread on day 1. The morphology of the cells changed significantly after 5 days of cultivation in differentiation medium, and most cells completely spread in a spindle shape. At the same time, N2a cells differentiated, and long synapses were observed in the 5 wt% GelMA and G:P=4:1 groups. However, cells in the G:P=2.5:2.5 group were not as spread out as in the other two groups, which can be attributed to the high PEGDA ratio not providing a biological ligand for cell adhesion, as we mentioned above.

Immunocytochemical staining and RT-qPCR were further used to evaluate the degree of cell differentiation and gene expression using the following three representative biomarkers: nestin, a neural progenitor marker for undifferentiated neural stem cells; βIII-Tubulin (Tuj-1), a tubulin protein expressed in neurons which plays a key role in normal axon guidance and maintenance [61]; and GFAP, an astrocyte-expressed glial fibrillary acidic protein which can be used as an astrocyte marker [62]. As shown in Fig. 3b, N2a cells were spherical without neurite outgrowth, and only slight signals of the neural differentiation markers (GFAP, Tuj-1) were present around the nucleus in all groups on day 1, while neural differentiation markers were significantly expressed with obvious neurite growth both in the control group and the hydrogel groups on day 5. We then quantified the neurite length, as shown in Fig. 3c1; the neurite length was calculated using ImageJ software (Simple Neurite Tracer) by tracing each individual neuron and its total neurite length [63]. From the data, the neurite growth of the GelMA group is much more apparent; neurite length decreased as more PEGDA was incorporated, and we attribute this to the increasingly weak cell adhesion due to the lack of RGD peptide. From Fig. 3c, one can see that the quantitative gene expression of nestin was lowest in the control group, where it increased along with increasing PEGDA concentration. Meanwhile, GFAP (a marker for astrocytes) was considerably more evident on the stiffer hydrogel group (lower PEGDA concentration) (Figs. 3b and 3c3), in contrast to the expression of Tuj-1 (Fig. 3c4). These data all agree with the literature by demonstrating that a stiffer hydrogel mechanical environment makes neural stem cells slightly more prone to astrocyte differentiation [37, 64-66]. We also noticed that while there was no significant difference between the GelMA group and the G:P=4:1 group in terms of neural marker expression, there was lower expression in both Tuj-1 and GFAP in the G:P=2.5:2.5 group. Again, this was likely due to the weaker cell adhesion of the hydrogel with a higher PEGDA concentration.
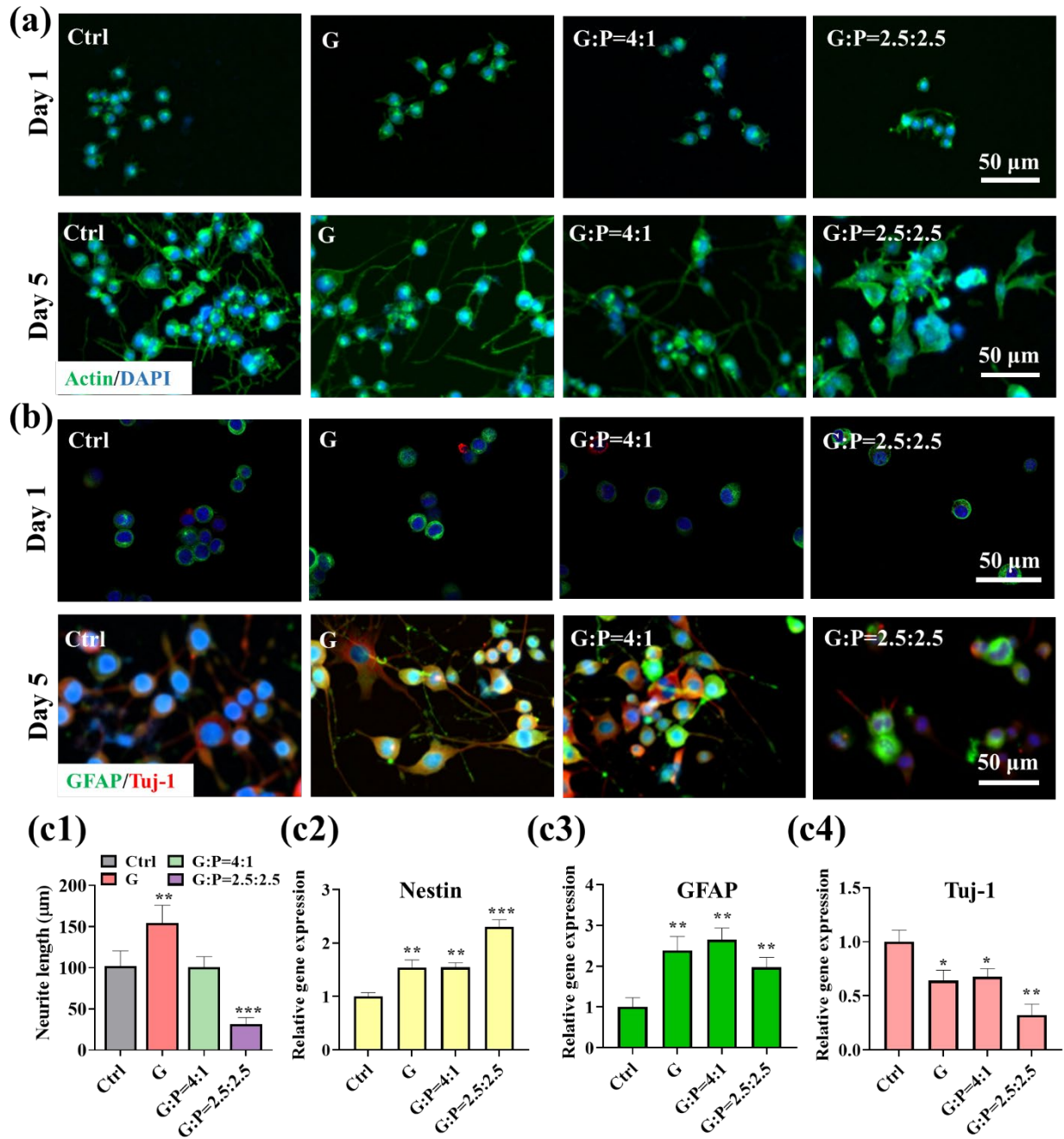
Fig. 3 Effect of hydrogel stiffness on N2a differentiation on 2D hydrogel. (a) Cell morphology by F-actin staining on day 1 and day 5. (b) Immunofluorescence staining on day 1 and day 5. (c1–c4) Neurite length and RT-qPCR analysis of neural differentiation-related gene expression on day 5 (yellow represents nestin; green represents GFAP; red represents Tuj-1). Ctrl: N2a cultured on a 12-well plate; G means 5 wt% GelMA; G:P=4:1 means 4 wt% GelMA+1 wt% PEGDA; G:P=2.5:2.5 means 2.5 wt% GelMA+2.5 wt% PEGDA.

3.4 Cell viability, proliferation, and differentiation in 3D hydrogels

After we confirmed that 2D hydrogels were indeed effective, we were able to evaluate whether the same applied in 3D hydrogels. To confirm the viability of the cells in the 3D hydrogel, we

performed live/dead staining on the 3D encapsulated cells. From Fig. 4a1, one can see that most cells were alive in all hydrogels, with almost no dead cells on day 1, and the cells were able to proliferate and form cell clusters after 5 days of cultivation, indicating the relatively high biocompatibility of GelMA-PEGDA hydrogels for 3D cell encapsulation. CCK-8 was used to quantitatively evaluate cell proliferation. As shown in Fig. 4a2, the proliferation of encapsulated N2a cells in all hydrogels was remarkably increased with culture time from day 1 to day 5. Also, similar to 2D hydrogels, cell proliferation in the G:P=2.5:2.5 group was relatively low compared with the 5 wt% GelMA group and the G:P=4:1 group, which again is likely due to having more PEGDA incorporated and hence lesser RGD peptide, as discussed above. We observed cell morphology in 3D hydrogels with a bright-field microscope (Fig. 4b). Compared with 2D hydrogels, cell differentiation in 3D hydrogels was significantly reduced and also seems to be different. Specifically, the cell morphology was slightly different between the GelMA group and the PEGDA group (G:P=4:1 and G:P=2.5:2.5), with cells in GelMA being round and having more synapses (indicating differentiation into glial cells), and the morphology of cells in the PEGDA group being more fusiform (indicating differentiation into neuronal cells). To confirm our observation, immunofluorescence staining and RT-qPCR were used to evaluate cell differentiation and gene expression in 3D hydrogel after 5 days of culture. As shown in the immunofluorescence data (Figs. 4c and 4d), there was higher green fluorescence (GFAP) in GelMA hydrogels and higher red fluorescence (Tuj-1) in GelMA-PEGDA hydrogels. This was consistent with our observations from cell morphology. Such discrepancies compared to the results of 2D hydrogels could be attributed to neural stem cells being more sensitive to stiffness than RGD content in a 3D environment [67], so that the stiffer hydrogel environment (GelMA) is more conducive to differentiation of glial cells, while the softer environment (GelMA-PEGDA) is more conducive to differentiation of neuronal cells [37, 65, 68]. In fact, these results also correspond to those from other studies where neural differentiation was significantly influenced by material stiffness in a 3D environment [37, 69]. As for the reduced differentiation in the 3D hydrogels compared to the 2D hydrogels, this could imply that neural differentiation requires much more delicate regulation in a mimicking microenvironment such as the 3D hydrogels. We thus further investigated the effect of mechanical stimulation (i.e., stretching) on neural differentiation in a 3D environment.
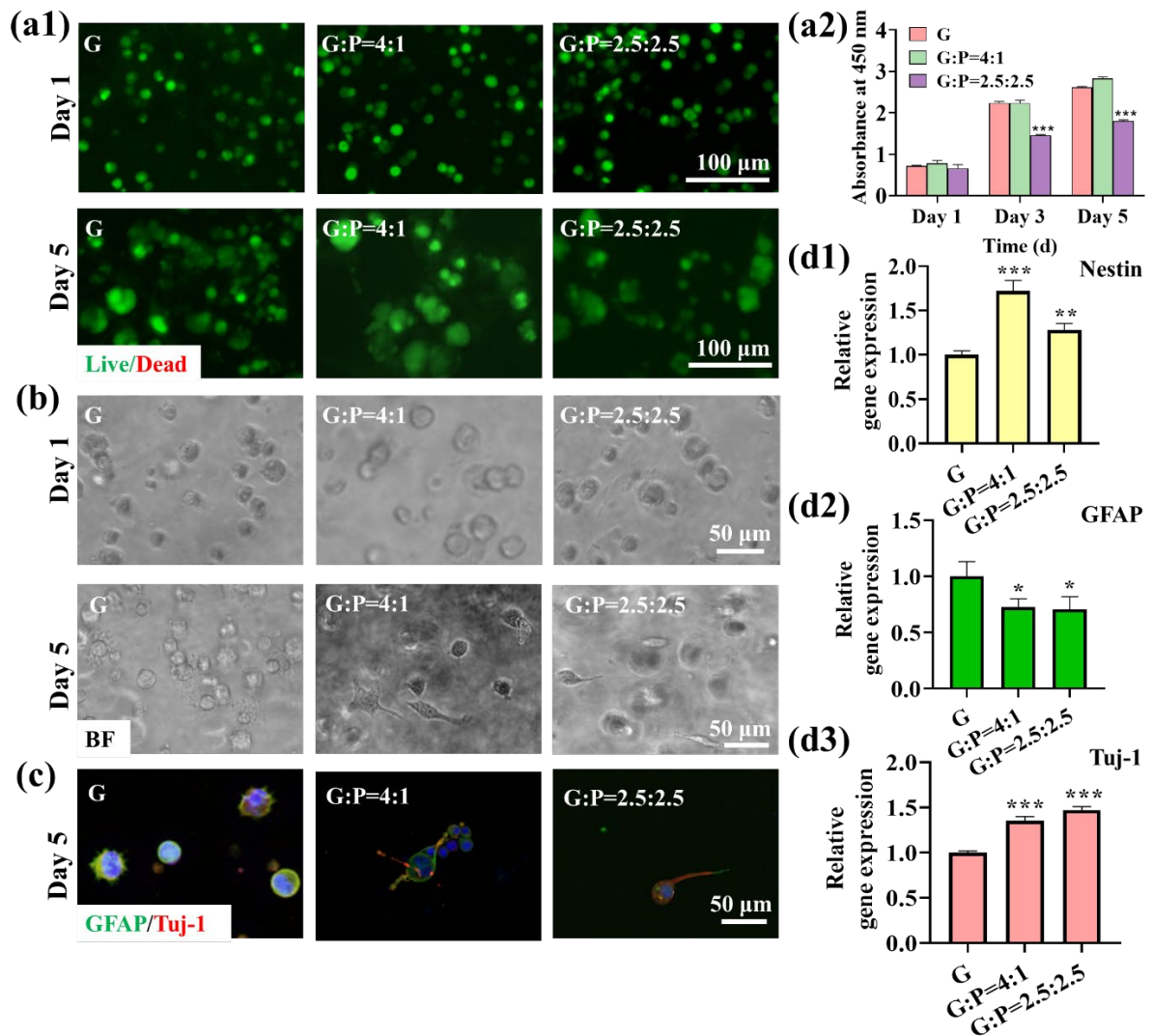
Fig. 4 Effect of hydrogel stiffness on N2a differentiation in 3D hydrogels. (a1) Live/dead staining on day 1 and day 5. (a2) Cell proliferation in 3D hydrogel. (b) Cell morphology on day 1 and day 5. (c) Immunofluorescence staining on day 5. (d1–d3) RT-qPCR analysis of neural differentiation-related gene expression on day 5 (yellow represents nestin; green represents GFAP; red represents Tuj-1). G means 5 wt% GelMA; G:P=4:1 means 4 wt% GelMA+1 wt% PEGDA; G:P=2.5:2.5 means 2.5 wt% GelMA+2.5 wt% PEGDA.

3.5 Effect of stretching 3D hydrogels on N2a differentiation
3.5.1 Effect of stretching 3D GelMA hydrogel on N2a differentiation

We investigated GelMA hydrogels undergoing 0%, 25%, and 50% of stretch from their original length, as shown in Fig. 5. Live/dead assay showed that cells still had high activity in stretched hydrogels on day 1 (Fig. 5a). Although some dead cells were observed, most of the cells were still alive, demonstrating the negligible effect of stretching on the viability of the encapsulated cells in the hydrogel. We observed cell morphology in 3D hydrogel after stretching, with bright-field microscopy (Fig. 5b). Compared with the unstretched hydrogels, the cells in the stretched hydrogels had more synaptic structures and longer axons (red arrows in Fig. 5b) as the stretching ratio increased (25% versus 50% stretching ratio), which was especially evident on

day 5. Specifically, the cells were round and did not show much neurite outgrowth on day 1, but the cell pseudopodia showed obvious elongation on day 5, especially for the stretching group. Again, most cells were in glial cell form in GelMA hydrogel since they were susceptible to glial differentiation in the slightly stiffer environment (7–10 kPa) [68].

Immunocytochemistry and quantitative gene expression examination was also conducted to study the effect of mechanical stimulation on neural differentiation in stretching and non-stretching GelMA hydrogel. GFAP and βIII-tubulin were selected as specific markers of glial cells and neuronal cells, respectively. Compared with the non-stretching group, longer neurite length was observed with an increase of stretching ratio (Fig. 5c). Based on the results of RT-qPCR, the relative gene expression of GFAP (2.3-fold) and βIII-tubulin (1.5-fold) was significantly increased in the stretched hydrogel compared with the non-stretched one, suggesting that mechanical stimulation could promote differentiation of N2a. Furthermore, expression of GFAP (a marker of glial cells) increased more than βIII-tubulin (a marker neuronal cell) after stretching, probably as a result of the higher modulus (stiffness) of GelMA hydrogel.
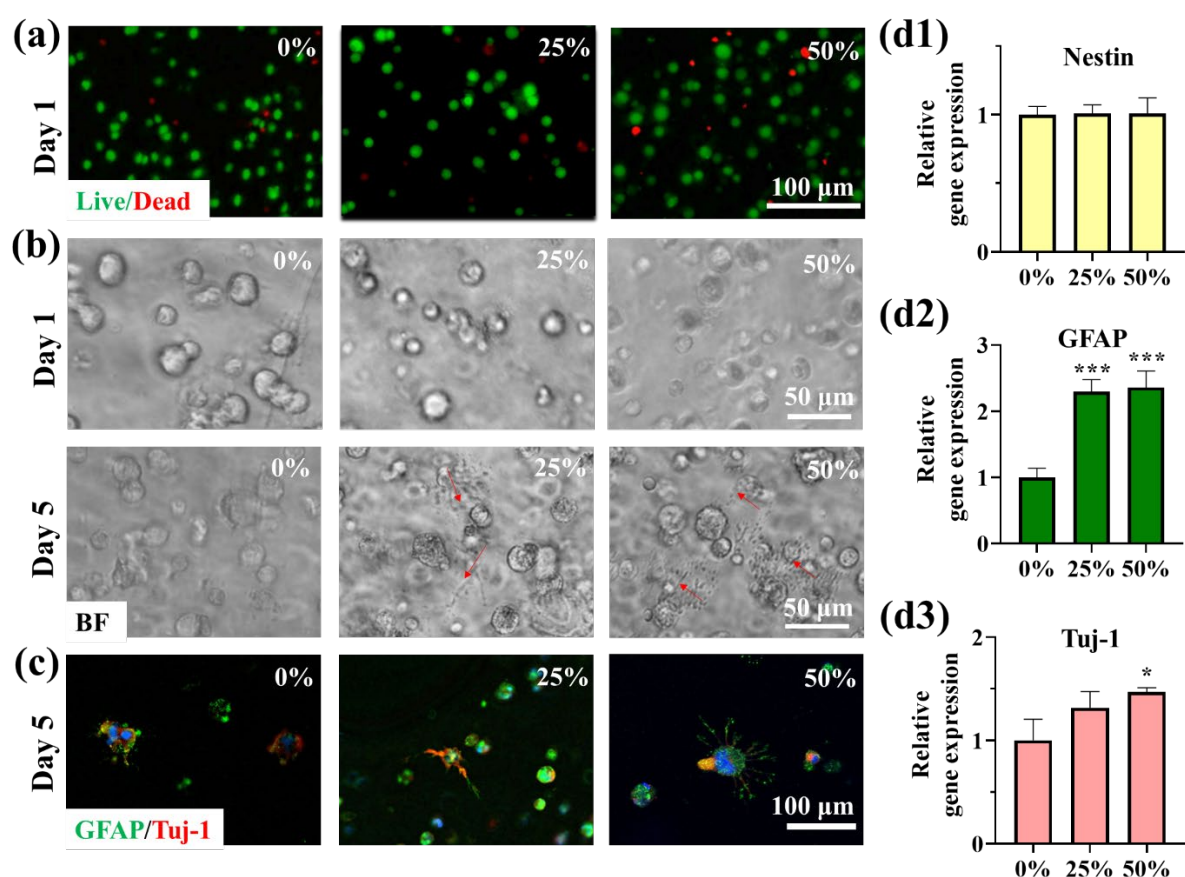

Fig. 5 Effect of stretching 3D G (5 wt% GelMA) hydrogel on N2a differentiation. (a) Live/dead staining on day 1. (b) Cell morphology on days 1 and 5. (c) Immunofluorescence staining on day 5. (d1–d3) RT-qPCR analysis of neural-differentiation-related gene expression on day 5 (yellow represents nestin; green represents GFAP; red represents Tuj-1). 0% means 0% stretching ratio; 25% means 25% stretching ratio; 50% means 50% stretching ratio.

3.5.2 Effect of stretching 3D GelMA-PEGDA hydrogel on N2a differentiation

16

In addition to stretching GelMA hydrogels, we stretched GelMA-PEGDA hydrogels (G:P=4:1 and G:P=2.5:2.5), as shown in Fig. 6. Most of the cells maintained high viability after stretching (Figs. 6a1 and 6a2). The morphology of N2a cells after stretching was imaged with microscopy on day 1 and day 5 (Figs. 6b1 and 6b2). Almost no neurite outgrowth was observed on day 1, but much more significant cell neurite development was seen after 5 days of culture compared to the GelMA group. Interestingly, stretching induced significant neurite outgrowth with longer neurites than the unstretched control group. Most notably, neurites grew randomly in the 0% stretched hydrogels on day 5 (Figs. 6c1 and 6c2), but showed more directional orientation in the stretching counterparts. That is, the orientation of neurite extension tended to follow the direction parallel to the mechanical tension in the stretched hydrogels, instead of exhibiting the random outgrowth seen in the non-stretching groups.

These observations were further confirmed by immunocytochemistry (Figs. 6c1 and 6c2). Elongated neuron growth was observed in the stretched GelMA-PEGDA hydrogels compared to the non-stretched one. Also, neurite elongation displayed a growth orientation that coincided with tensile force. Meanwhile, the intensity of Tuj-1 (red), a neuronal differentiation marker, was increased in the stretching group. To further evaluate relative gene expression, RT-qPCR was complemented to quantify it (Figs. 6d1–6d6). In concordance with the immunofluorescence results, the relative gene expression of GFAP and Tuj-1 was about 3-fold and 2-fold higher in the stretched GelMA-PEGDA hydrogel than the control after 5 days of culture. These results clearly demonstrated that the mechanical tension apparently influences neural differentiation towards neurons under stretching conditions, especially when the hydrogels are sufficiently flexible. The differentiation of 3D-encapsulated neural cells was significantly influenced by their 3D environment. On the one hand, cells cultivated in the stiffer hydrogel were more likely to differentiate into glial cells, while cells encapsulated in the soft hydrogel were more prone to differentiation into neuronal cells. On the other hand, mechanical stretching further enhanced neural differentiation by promoting neurite extension and axon elongation.
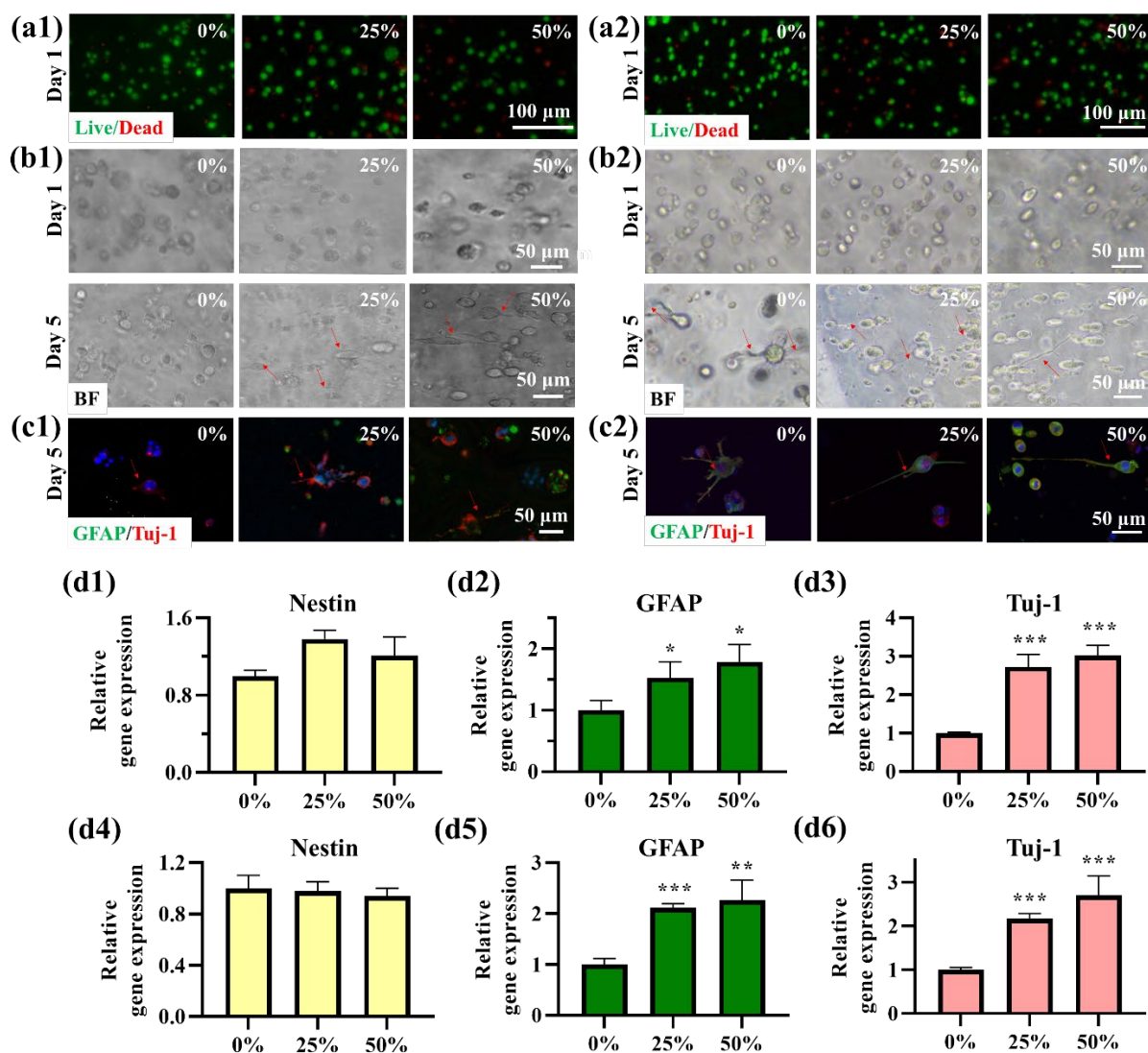
Fig. 6 Effect of stretching 3D GelMA-PEGDA hydrogel on N2a differentiation. (a) Live/dead staining on day 1 for GelMA-PEGDA hydrogel G:P=4:1 (a1) and G:P=2.5:2.5 (a2). (b) Cell morphology on day 1 and day 5 for GelMA-PEGDA hydrogel G:P=4:1 (b1) and G:P=2.5:2.5 (b2). (c) Immunofluorescence staining on day 5 for GelMA-PEGDA hydrogel G:P=4:1 (c1) and G:P=2.5:2.5 (c2). (d1–d6) RT-qPCR analysis of neural differentiation-related gene expression on day 5 for GelMA-PEGDA hydrogel G:P=4:1 (d1–d3) and G:P=2.5:2.5 (d4–d6) (yellow represents nestin; green represents GFAP; red represents Tuj-1). 0% means 0% stretching ratio; 25% means 25% stretching ratio; 50% means 50% stretching ratio. G:P=4:1 represents 4 wt% GelMA+1 wt% PEGDA and G:P=2.5:2.5 represents 2.5 wt% GelMA+2.5 wt% PEGDA.

Conclusions

In conclusion, we successfully prepared soft and stretchable GelMA-PEGDA hydrogels to create favorable 3D mimicking microenvironments for neural cell culture. By incorporating PEGDA into the biocompatible GelMA polymer and varying its concentration, we were able to not only regulate the matrix stiffness of hydrogels, but also enhance the tensile properties of the hydrogels in general. Although the addition of PEGDA slightly influenced cell viability and

18

proliferation due to the lack of the RGD group, GelMA-PEGDA still has the extremely high biocompatibility needed for 3D neural cells to thrive. Meanwhile, stem cells are more favorable for glial cell differentiation with high GFAP protein expression in GelMA hydrogel (~5.8 kPa), and more favorable for neuronal cell differentiation with high Tuj-1 protein expression in GelMA-PEGDA hydrogel (0.8–2.8 kPa) with a higher PEGDA concentration. This can be mostly attributed to the change of stiffness even under also changes in concentration of RGD peptides. In fact, both the decrease in RGD peptide concentration and the stiffness play a similar role in discouraging cell adhesion to that suggested by a landmark study [70], while neural stem cells are also especially sensitive to stiffness. Neural differentiation is significantly influenced by the mechanical modulus of 3D hydrogels compared to the changes in concentration of RGD peptides, as shown in other studies [67]. This suggests that stiffness plays the dominant role in regulating neuronal cell differentiation, as is shown by our data and consistent with many other studies [37, 69]. Furthermore, we show that 3D neural differentiation could be enhanced by mechanical tensions in terms of axon elongation and neurite orientation. Altogether, the data suggest that mechanical stretching in a 3D hydrogel microenvironment improves neurogenesis in general, agreeing not only with current knowledge of in vivo neural mechanical niches, but also demonstrating that GelMA-PEGDA hydrogel encapsulation and stretching are possible strategies to improve efficacy and viability of neural stem cell therapies for regenerative medicine.

Author contributions

XZ was involved in conceptualization, funding acquisition, supervision, and writing–review & editing. QM contributed to the investigation, methodology, data curation, formal analysis, visualization, and writing—original draft, review & editing. HYY helped in writing—original draft, review & editing.

Declarations

Conflict of interest

The authors declare that they have no conflict of interest.

Ethical approval

This article does not contain any studies with human or animal subjects performed by any of the authors.

References

1. Toyama BH, Savas JN, Park SK, et al (2013) Identification of long-lived proteins reveals exceptional stability of essential cellular structures. Cell 154(5):971-982.

https://doi.org/10.1016/j.cell.2013.07.037

2. Keung AJ, Asuri P, Kumar S, et al (2012) Soft microenvironments promote the early neurogenic differentiation but not self-renewal of human pluripotent stem cells. Integrat Biol. 4(9):1049-1058. https://doi.org/10.1039/c2ib20083j

3. Van Essen DC (1997) A tension-based theory of morphogenesis and compact wiring in the central nervous system. Nature 385(6614):313-318. https://doi.org/10.1038/385313a0

4. Mothe AJ, Tator CH (2013) Review of transplantation of neural stem/progenitor cells for spinal cord injury. Int J Develop Neurosci 31(7):701-713. https://doi.org/10.1007/s42242-020-00089-1

5. Kojima K, Miyoshi H, Nagoshi N, et al (2019) Selective ablation of tumorigenic cells following human induced pluripotent stem cell-derived neural stem/progenitor cell transplantation in spinal cord injury. Stem Cells Transl Med 8(3):260-270. https://doi.org/10.1002/sctm.18-0096

6. Thakor J, Ahadian S, Niakan A, et al (2020) Engineered hydrogels for brain tumor culture and therapy. Bio-Des Manuf 3(3):203-226. https://doi.org/10.1007/s42242-020-00084-6

7. Béduer A, Vieu C, Arnauduc F, et al (2012) Engineering of adult human neural stem cells differentiation through surface micropatterning. Biomaterials 33(2):504-514. https://doi.org/10.1016/j.biomaterials.2011.09.073

8. Zhang D, Suo H, Qian J, et al (2020) Physical understanding of axonal growth patterns on grooved substrates: groove ridge crossing versus longitudinal alignment. Bio-Des Manuf 3(4):348-360. https://doi.org/10.1007/s42242-020-00089-1

9. Chen JWE, Pedron S, Harley BA (2017) The combined influence of hydrogel stiffness and matrix-bound hyaluronic acid content on glioblastoma invasion. Macromol Biosci 17(8):1700018. https://doi.org/10.1002/mabi.201700018

10. Heffernan JM, Overstreet DJ, Le LD, et al (2015) Bioengineered scaffolds for 3D analysis of glioblastoma proliferation and invasion. Ann Biomed Eng 43(8):1965-1977. https://doi.org/10.1007/s10439-014-1223-1

11. Riehl BD, Park JH, Kwon IK, et al (2012) Mechanical stretching for tissue engineering: two-dimensional and three-dimensional constructs. Tissue Eng Part B Rev 18(4):288-300. https://doi.org/10.1089/ten.teb.2011.0465

12. Tyler WJJNRN (2012) The mechanobiology of brain function. Nat Rev Neurosci 13(12):867-878. https://doi.org/10.1038/nrn3383

13. Guimarães CF, Gasperini L, Marques AP, et al (2020) The stiffness of living tissues and its implications for tissue engineering. Nat Rev Mater 5(5):351-370. https://doi.org/10.1038/s41578-019-0169-1

14. McGlynn E, Nabaei V, Ren E, et al (2021) The future of neuroscience: flexible and wireless implantable neural electronics. Adv Sci 8(10):2002693. https://doi.org/10.1002/advs.202002693

15. Holtzmann K, Gautier HO, Christ AF, et al (2016) Brain tissue stiffness is a sensitive marker for acidosis. J Neurosci Methods 271:50-54. https://doi.org/10.1016/j.jneumeth.2016.07.002

16. Jorba I, Menal MJ, Torres M, et al (2017) Ageing and chronic intermittent hypoxia mimicking sleep apnea do not modify local brain tissue stiffness in healthy mice. J Mech Behav Biomed Mater 71:106-113. https://doi.org/10.1016/j.jmbbm.2017.03.001

17. Murphy MC, Jones DT, Jack Jr CR, et al (2016) Regional brain stiffness changes across the Alzheimer's disease spectrum. NeuroImage Clin 10:283-290. https://doi.org/10.1016/j.nicl.2015.12.007

18. Kolipaka A, Wassenaar PA, Cha S, et al (2018) Magnetic resonance elastography to estimate brain stiffness: measurement reproducibility and its estimate in pseudotumor cerebri patients. Clin Imag 51:114-122. https://doi.org/10.1016/j.clinimag.2018.02.005

19. Arani A, Murphy MC, Glaser KJ, et al (2015) Measuring the effects of aging and sex on regional brain stiffness with MR elastography in healthy older adults. Neuroimage 111:59-64. https://doi.org/10.1016/j.neuroimage.2015.02.016

20. Handorf AM, Zhou Y, Halanski MA, et al (2015) Tissue stiffness dictates development, homeostasis, and disease progression. Organogenesis 11(1):1-15. https://doi.org/10.1080/15476278.2015.1019687

21. Saxena T, Gilbert J, Stelzner D, et al (2012) Mechanical characterization of the injured spinal cord after lateral spinal hemisection injury in the rat. J Neurotrauma 29(9):1747-1757. https://doi.org/10.1089/neu.2011.1818

22. Saxena T, Gilbert JL, Hasenwinkel JM (2009) A versatile mesoindentation system to evaluate the micromechanical properties of soft, hydrated substrates on a cellular scale. J Biomed Mater Res Part A 90(4):1206-1217. https://doi.org/10.1002/jbm.a.32178

23. Ozawa H, Matsumoto T, Ohashi T, et al (2001) Comparison of spinal cord gray matter and white matter softness: measurement by pipette aspiration method. J Neurosurg Spine 95(2):221-224. https://doi.org/10.3171/spi.2001.95.2.0221

24. Nachlas AL, Li S, Jha R, et al (2018) Human iPSC-derived mesenchymal stem cells encapsulated in PEGDA hydrogels mature into valve interstitial-like cells. Acta Biomater 71:235-246. https://doi.org/10.1016/j.actbio.2018.02.025

25. Weber LM, He J, Bradley B, et al (2006) PEG-based hydrogels as an in vitro encapsulation platform for testing controlled β-cell microenvironments. Acta Biomater 2(1):1-8. https://doi.org/10.1016/j.actbio.2005.10.005

26. Han WT, Jang T, Chen S, et al (2020) Improved cell viability for large-scale biofabrication with photo-crosslinkable hydrogel systems through a dual-photoinitiator approach. Biomater Sci 8(1):450-461. 10.1039/C9BM01347D

27. Ying J, Han Z, Zeng Y, et al (2019) Evaluation of intervertebral disc regeneration with injection of mesenchymal stem cells encapsulated in PEGDA-microcryogel delivery system using quantitative T2 mapping: a study in canines. Am J Transl Res 11(4):2028-2041.

28. Xiao S, Zhao T, Wang J, et al (2019) Gelatin methacrylate (GelMA)-based hydrogels for cell transplantation: an effective strategy for tissue engineering. Stem Cell Rev Rep 15(5):664-679. https://doi.org/10.1007/s12015-019-09893-4

29. Zhao X, Liu S, Yildirimer L, et al (2016) Injectable stem cell-laden photocrosslinkable microspheres fabricated using microfluidics for rapid generation of osteogenic tissue constructs. Adv Funct Mater 26(17):2809-2819. https://doi.org/10.1002/adfm.201504943

30. Koffler J, Zhu W, Qu X, et al (2019) Biomimetic 3D-printed scaffolds for spinal cord injury repair. Nat Med 25(2):263-269. https://doi.org/10.1038/s41591-018-0296-z

31. Zhang X, Xu B, Puperi DS, et al (2015) Integrating valve-inspired design features into poly (ethylene glycol) hydrogel scaffolds for heart valve tissue engineering. Acta Biomater 14:11-21. https://doi.org/10.1016/j.actbio.2014.11.042

32. Wang Y, Cao X, Ma M, et al (2020) A GelMA-PEGDA-nHA composite hydrogel for bone tissue engineering. Materials 13(17):3735. https://doi.org/10.3390/ma13173735

33. Skaalure SC, Chu S, Bryant SJ (2015) An enzyme-sensitive PEG hydrogel based on aggrecan catabolism for cartilage tissue engineering. Adv Healthcare Mater 4(3):420-431. https://doi.org/10.1002/adhm.201400277

34. Sun M, Sun X, Wang Z, et al (2018) Synthesis and properties of gelatin methacryloyl (GelMA) hydrogels and their recent applications in load-bearing tissue. Polymers 10(11):1290. https://doi.org/10.3390/polym10111290

35. Ying G, Jiang N, Yu C, et al (2018) Three-dimensional bioprinting of gelatin methacryloyl (GelMA). Bio-Des Manuf 1(4):215-224. https://doi.org/10.1007/s42242-018-0028-8

36. Liu Y, Chan-Park MB (2010) A biomimetic hydrogel based on methacrylated dextran-graft-lysine and gelatin for 3D smooth muscle cell culture. Biomaterials 31(6):1158-1170. https://doi.org/10.1016/j.biomaterials.2009.10.040

37. Fan L, Liu C, Chen X, et al (2018) Directing induced pluripotent stem cell derived neural stem cell fate with a three-dimensional biomimetic hydrogel for spinal cord injury repair. ACS Appl Mater Interf 10(21):17742-17755. https://doi.org/10.1021/acsami.8b05293

38. Pathak MM, Nourse JL, Tran T, et al (2014) Stretch-activated ion channel Piezo1 directs lineage choice in human neural stem cells. Proc Natl Acad Sci 111(45):16148-16153. https://doi.org/10.1073/pnas.1409802111

39. Suzuki M, Morita H, Ueno N (2012) Molecular mechanisms of cell shape changes that contribute to vertebrate neural tube closure. Develop Growth Differ 54(3):266-276. https://doi.org/10.1111/j.1440-169X.2012.01346.x

40. Zhao X, Lang Q, Yildirimer L, et al (2016) Photocrosslinkable gelatin hydrogel for epidermal tissue engineering. Adv Healthcare Mater 5(1):108-118. https://doi.org/10.1002/adhm.201500005

41. Son KH, Lee JWJM (2016) Synthesis and characterization of poly (ethylene glycol) based thermo-responsive hydrogels for cell sheet engineering. Materials 9(10):854. https://doi.org/10.3390/ma9100854

42. Zhang L, Zhao J, Zhu J, et al (2012) Anisotropic tough poly (vinyl alcohol) hydrogels. Soft Matter 8(40):10439-10447. https://doi.org/10.1039/C2SM26102B

43. Gan D, Huang Z, Wang X, et al (2020) Graphene oxide-templated conductive and redox-active nanosheets incorporated hydrogels for adhesive bioelectronics. Adv Funct Mater 30(5):1907678. https://doi.org/10.1002/adfm.201907678

44. Zhu M, Wang Y, Ferracci G, et al (2019) Gelatin methacryloyl and its hydrogels with an exceptional degree of controllability and batch-to-batch consistency. Sci Rep 9(1):1-13. https://doi.org/10.1038/s41598-019-42186-x

45. Park J, Jeon J, Kim B, et al (2020) Electrically conductive hydrogel nerve guidance conduits for peripheral nerve regeneration. Adv Funct Mater 30(39):2003759. https://doi.org/10.1002/adfm.202003759

46. Tremblay RG, Sikorska M, Sandhu JK, et al (2010) Differentiation of mouse Neuro 2A cells into dopamine neurons. J Neurosci Methods 186(1):60-67. https://doi.org/10.1016/j.jneumeth.2009.11.004

47. Namsi A, Nury T, Hamdouni H, et al (2018) Induction of neuronal differentiation of murine N2a cells by two polyphenols present in the mediterranean diet mimicking neurotrophins

activities: resveratrol and apigenin. Diseases 6(3):67. https://doi.org/10.3390/diseases6030067

48. Yang Y, Xu T, Zhang Q, et al (2021) Biomimetic, stiff, and adhesive periosteum with osteogenic–angiogenic coupling effect for bone regeneration. Small 17(14):2006598. https://doi.org/10.1002/smll.202006598

49. Li W, Fan X, Wang Y, et al (2020) A glycidyl methacrylate modified collagen/polyethylene glycol diacrylate hydrogel: a mechanically strong hydrogel for loading levofloxacin. New J Chem 44(39):17027-17032. https://doi.org/10.1039/D0NJ02853C

50. Imani M, Sharifi S, Mirzadeh H, et al (2007) Monitoring of polyethylene glycoldiacrylate-based hydrogel formation by real time NMR spectroscopy. Iranian Polym J 16(1):14-20.

51. Abramowitch S, Easley D (2016) Introduction to classical mechanics. In: Hoyte L, Damaser M (Eds.), Biomechanics of the Female Pelvic Floor. Academic Press, USA. p.89-107. https://doi.org/10.1016/B978-0-12-803228-2.00004-0

52. Della Sala F, Biondi M, Guarnieri D, et al (2020) Mechanical behavior of bioactive poly (ethylene glycol) diacrylate matrices for biomedical application. J Mech Behav Biomed Mater 110:103885. https://doi.org/10.1016/j.jmbbm.2020.103885

53. Temenoff JS, Athanasiou KA, Lebaron RG, et al (2002) Effect of poly (ethylene glycol) molecular weight on tensile and swelling properties of oligo (poly (ethylene glycol) fumarate) hydrogels for cartilage tissue engineering. J Biomed Mater Res 59(3):429-437. https://doi.org/10.1002/jbm.1259

54. Sun H, Haque FM, Zhang Y, et al (2019) Linear-dendritic alternating copolymers. Angewandte Chemie 131(31):10682-10686. https://doi.org/10.1002/ange.201903402

55. Cantini M, Donnelly H, Dalby MJ, et al (2020) The plot thickens: the emerging role of matrix viscosity in cell mechanotransduction. Adv Healthcare Mater 9(8):1901259. https://doi.org/10.1002/adhm.201901259

56. Murrell M, Kamm R, Matsudaira P (2011) Substrate viscosity enhances correlation in epithelial sheet movement. Biophys J 101(2):297-306. https://doi.org/10.1016/j.bpj.2011.05.048

57. Fernández-Pérez J, Ahearne M (2019) The impact of decellularization methods on extracellular matrix derived hydrogels. Sci Rep 9(1):1-12. 10.1016/j.actbio.2018.02.025

58. Stillman Z, Jarai BM, Raman N, et al (2020) Degradation profiles of poly (ethylene glycol) diacrylate (PEGDA)-based hydrogel nanoparticles. Polym Chem 11(2):568-580. https://doi.org/10.1039/C9PY01206K

59. Browning M, Cereceres S, Luong P, et al (2014) Determination of the in vivo degradation mechanism of PEGDA hydrogels. J Biomed Mater Res Part A 102(12):4244-4251. https://doi.org/10.1002/jbm.a.35096

60. Jia J, Coyle RC, Richards DJ, et al (2016) Development of peptide-functionalized synthetic hydrogel microarrays for stem cell and tissue engineering applications. Acta Biomater 45:110-120. https://doi.org/10.1016/j.actbio.2016.09.006

61. Oyarce K, Silva-Alvarez C, Ferrada L, et al (2018) SVCT2 is expressed by cerebellar precursor cells, which differentiate into neurons in response to ascorbic acid. Molec Neurobiol 55(2):1136-1149. https://doi.org/10.1007/s12035-016-0366-5

62. Philip DL, Silantyeva EA, Becker ML, et al (2019) RGD-functionalized nanofibers increase early GFAP expression during neural differentiation of mouse embryonic stem cells. Biomacromolecules 20(3):1443-1454. https://doi.org/10.1021/acs.biomac.9b00018

63. Jin J, Tilve S, Huang Z, et al (2018) Effect of chondroitin sulfate proteoglycans on neuronal cell adhesion, spreading and neurite growth in culture. Neur Regener Res 13(2):289. https://doi.org/10.4103/1673-5374.226398

64. Hsieh FY, Tseng TC, Hsu SH (2015) Self-healing hydrogel for tissue repair in the central nervous system. Neur Regener Res 10(12):1922. https://doi.org/10.4103/1673-5374.169624

65. Banerjee A, Arha M, Choudhary S, et al (2009) The influence of hydrogel modulus on the proliferation and differentiation of encapsulated neural stem cells. Biomaterials 30(27):4695-4699. https://doi.org/10.1016/j.biomaterials.2009.05.050

66. Zhu Y, Li X, Janairo RRR, et al (2019) Matrix stiffness modulates the differentiation of neural crest stem cells in vivo. J Cellular Physiol 234(5):7569-7578. https://doi.org/10.1002/jcp.27518

67. Stukel JM, Willits RK (2018) The interplay of peptide affinity and scaffold stiffness on neuronal differentiation of neural stem cells. Biomed Mater 13(2):024102. 10.1088/1748-605X/aa9a4b

68. Tseng TC, Tao L, Hsieh FY, et al (2015) An injectable, self-healing hydrogel to repair the central nervous system. Adv Mater 27(23):3518-3524. https://doi.org/10.1002/adma.201500762

69. Wu S, Xu R, Duan B, et al (2017) Three-dimensional hyaluronic acid hydrogel-based models for in vitro human iPSC-derived NPC culture and differentiation. J Mater Chem B 5(21):3870-3878. https://doi.org/10.1039/C7TB00721C

70. Ye K, Wang X, Cao L, et al (2015) Matrix stiffness and nanoscale spatial organization of cell-adhesive ligands direct stem cell fate. Nano Lett 15(7):4720-4729. https://doi.org/10.1021/acs.nanolett.5b01619